

Hybridization-switching induced Mott transition in ABO₃ perovskites

Atanu Paul,¹ Anamitra Mukherjee,² Indra Dasgupta,¹ Arun Paramakanti,³ and Tanusri Saha-Dasgupta^{4,5,*}

¹*Department of Solid State Physics, Indian Association for the Cultivation of Science, Kolkata 700 032, India.*

²*School of Physical Sciences, National Institute of Science Education and Research, HBNI, Jatni 752050, India.*

³*Department of Physics, University of Toronto, Toronto, Ontario, Canada M5S 1A7.*

⁴*Department of Condensed Matter Physics and Materials Science,
S.N. Bose National Centre for Basic Sciences, Kolkata 700098, India.*

⁵*Center for Mathematical, Computational and Data Science,
Indian Association for the Cultivation of Science, Kolkata 700 032, India.*

(Dated: January 21, 2019)

We propose the concept of “hybridization-switching induced Mott transition” which is relevant to a broad class of ABO₃ perovskite materials including BiNiO₃ and PbCrO₃ which feature extended 6s orbitals on the A-site cation (Bi or Pb), and A-O covalency induced ligand holes. Using *ab initio* electronic structure and slave rotor theory calculations, we show that such systems exhibit a breathing phonon driven A-site to oxygen hybridization-wave instability which conspires with strong correlations on the B-site transition metal ion (Ni or Cr) to induce a Mott insulator. These Mott insulators with active A-site orbitals are shown to undergo a pressure induced insulator to metal transition accompanied by a colossal volume collapse due to ligand hybridization switching.

Recent advances in transition metal oxides have led to a renewed interest in correlation driven metal-insulator transitions (MITs) [1–9]. Such MITs have been extensively explored in the ABO₃ perovskite family of materials, in which the A-site and B-site cations live on interpenetrating (nominally) cubic lattices. In typical perovskites, the A-site ion is passive, while the B-site transition metal (TM) ion actively dictates the electronic response. The A-site ion thus controls electronic properties only *indirectly*: its size tunes B-O-B bond angles and thus the B-electron bandwidth, while its charge determines the electron filling. For instance, experimental [10–26] and theoretical [27–37] studies of perovskite nickelates RNiO₃ (R being a rare-earth ion) have shown that varying R, with increasing ionic sizes, induces a Mott insulator to metal transition driven by an increase in the Ni bandwidth.

In significant contrast to the above scenario, recent experiments on BiNiO₃ [38] and PbCrO₃ [39], reveal a distinct behavior. BiNiO₃, with the large Bi cation at the A-site, is an insulator rather than a metal at ambient pressure [40]. This insulator becomes metallic at a critical pressure of 3.5 GPa, with a significant 2.5% volume contraction. Similarly PbCrO₃ exhibits an insulator-to-metal transition at 2.5 GPa [39] with a *colossal* 7.8% volume collapse! Similar large volume shrinking insulator-to-metal transitions have been observed upon heating; this technologically important phenomenon was termed “colossal negative thermal expansion” [41, 42].

For BiNiO₃, attempts to address its MIT using Hartree-Fock theory [43] and dynamical mean-field theory [44] have focused on models involving only Bi and Ni sites. These studies view the insulator as a checkerboard charge crystal $[\text{Bi}_{0.5}^{3+}\text{Bi}_{0.5}^{5+}][\text{Ni}^{2+}]$, assuming that Bi acts as a valence skipping ion with an attractive U Hubbard interaction, while the high pressure metal results from a

valence transition into a uniform $[\text{Bi}^{3+}][\text{Ni}^{3+}]$ configuration. However, photoemission spectroscopy on the metal [45, 46] reveals that the nickel valence state is far from being purely Ni³⁺. At the same time, Bi⁵⁺ has an energetically deep 6s shell [47] which strongly suppresses Bi³⁺-Bi⁵⁺ charge disproportionation. These theories neither discuss the crucial role of ligand nor that of the lattice in the MIT. These issues are reminiscent of the “charge disproportionation” debate in insulating RNiO₃ and B-site bismuthate BaBiO₃ [48–53]. Indeed, rather than being Ni²⁺-Ni³⁺ charge crystals, the RNiO₃ insulators feature a NiO₆ breathing mode instability, leading to site-selective Mott insulators; holes on one Ni sublattice undergo a Mott transition while holes on the other sublattice reside in NiO₆ molecular orbitals [30, 31, 48, 49].

In this Letter, we show that a natural solution to volume collapse MIT in TM ABO₃ with active A site emerges if the oxygen sites and lattice distortions are explicitly included in modelling these novel perovskites. In steps towards this, we first show, using density functional theory (DFT) on specific ABO₃ perovskites, BiNiO₃ and PbCrO₃, that the key to their phenomenology lies in an active A-site with 6s orbital which can strongly hybridize with oxygen, creating ligand holes. Based on this, we propose a simplified model for such perovskites which includes all three ions (A,B,O) and the lattice degree of freedom, and solve it using slave rotor theory. We find that as the oxygen energy level becomes close to that of A-site cation, driving a negative charge-transfer situation, the extended A-site orbital permits an A-O breathing mode instability, which leads to a three-dimensional (3D) checkerboard pattern of compressed and expanded AO₁₂ polyhedra. This is analogous to a 3D Peierls’ transition in a strongly correlated regime, which does not rely on Fermi surface nesting [54, 55]. This instability suppresses the B-O hybridization, triggering a Mott in-

ulating state due to strong correlations on the B-site ions. Applying pressure shifts the ligand energy, favoring B-O over A-O hybridization. This *hybridization-switch* eventually suppresses the A-O breathing mode instability and the concomitant hybridization-wave, leading to a metal dominated by B-O states at the Fermi level. Our results motivate us to conclude that BiNiO_3 and PbCrO_3 belong to a broad category of compounds exhibiting *hybridization-switching induced Mott transition*. We propose further material candidates in this category, namely TlMnO_3 and InMnO_3 .

Pressure-induced structural transition.— At ambient pressure (AP), the crystal structure of BiNiO_3 is triclinic, with two inequivalent Bi sites (Bi1, Bi2), and four inequivalent Ni sites. The high pressure (HP) phase, above 3.5 GPa [56], has orthorhombic symmetry, with equivalent Bi and Ni sites. The AP phase has a staggered pattern of compressed and expanded BiO_{12} polyhedra, while the HP phase features BiO_{12} polyhedra of uniform volume. We begin by describing this structural transition within DFT. DFT calculations were carried out in pseudo-potential plane-wave basis with generalized gradient approximation [57] with Hubbard U (GGA+ U) [58] ($U=4$ eV, $J_H=0.9$ eV), as implemented in Vienna-Abinitio-Simulation-Package [59]; see Supplemental Material (SM) for details [60].

We fit the volume dependence of our DFT cohesive energies of the AP (triclinic) and HP (orthorhombic) structures to the Birch-Murnaghan equation [61]. Using a common tangent construction (see Fig. 1 (a)), we find a transition from low-symmetry triclinic to high-symmetry orthorhombic structure with a volume reduction of $\approx 3\%$, in good agreement with high pressure experiments [42].

To understand the role of the bond deformation in the MIT, we computed the stiffness of the Bi-O bonds. Starting from the undistorted orthorhombic structure at volumes corresponding to AP and HP (at 6 GPa), and replacing Ni ions by a uniform positive background, we calculated the energy change δE for small breathing displacement of oxygen atoms (δO) from their equilibrium positions; see Fig. 1(b) inset. Fitting $\delta E = \frac{1}{2}k(\delta O)^2$ yields the Bi-O bond stiffness constants $k_{\text{BiO}} = 2.06 \text{eV}/\text{\AA}^2$ and $2.32 \text{eV}/\text{\AA}^2$ for AP and 6 GPa HP volumes, respectively. For the Ni-O sublattice, see Fig. 1(b), corresponding calculations yield $k_{\text{NiO}} = 7.96 \text{eV}/\text{\AA}^2$ and $10.84 \text{eV}/\text{\AA}^2$. Thus, the Ni-O bond, which is stiffer than Bi-O bond, becomes substantially stiffer at HP, suppressing a distortion of the Ni-O sublattice. For comparison, the similarly calculated Ni-O stiffness in PrNiO_3 , which shows a breathing mode distortion [62], is $7.22 \text{eV}/\text{\AA}^2$, a factor of 1.5 smaller than that of HP BiNiO_3 . This explains the absence of a breathing mode distortion of NiO_6 octahedra in the HP phase, and the resulting stability of the volume-collapsed metal against a Ni “charge-disproportionation” MIT.

DFT electronic structure.— Fig. 2(a) shows the spin-polarized GGA+ U density of states (DOS) of AP and

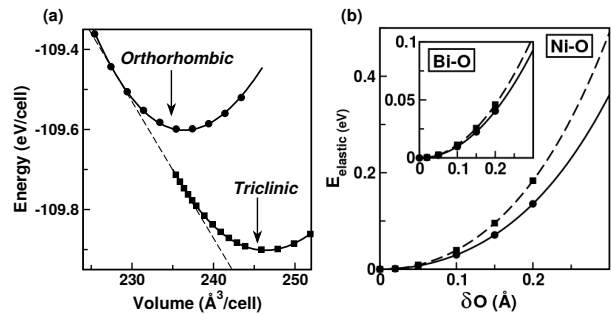


FIG. 1: (Color online) (a) DFT cohesive energy versus volume for AP (triclinic) and HP (orthorhombic) BiNiO_3 ; the intersection points of the plotted common tangent with the two curves yields the volume change $\Delta V/V \approx 3\%$ at the transition. (b) Elastic energy of Ni-O sublattice as a function of O-displacement for the HP (dashed) and AP (solid) volumes. Inset shows similar plot for Bi-O sublattice.

HP (7 GPa) BiNiO_3 , respectively, projected onto Bi- s , Ni- d and O- p states. The Ni- d and O- p plots are the DOS averaged over four inequivalent Ni sites in AP, and six and two O sites in AP and HP, respectively.

At AP, our DFT calculation gives rise to an insulating solution upon including antiferromagnetic (AFM) order. Both Bi1 and Bi2 sites show filled $6s$ states deep down in energy $\approx 10.5 \text{eV}$ below Fermi level (E_F). The split-off, unoccupied part of Bi2- s states, which is at $\approx 1 \text{eV}$ above E_F , and well-separated from the filled Bi2- s states by $\approx 9-10 \text{eV}$, is entirely derived from strong admixture with O- p states, signaling creation of ligand holes (see encircled regions in the figure). Thus, the insulator is *weakly* Bi-charge disproportionated [63]. The contribution of Ni- d to this split-off state is small. We find the Ni- d states are filled in the majority spin channel, while in the minority spin channel the octahedral crystal-field split Ni- t_{2g} and Ni- e_g states are respectively filled and empty (positioned beyond the energy shown in the figure). This suggests the stabilization of $[\text{Bi}_{1.5}^{3+}\text{Bi}_{0.5}^{2+}\text{O}_{0.5}^{2-}]_{0.5}[\text{Ni}^{2+}\text{O}_{0.5}^{2-}]$ configuration in AP, instead of the proposed $[\text{Bi}_{1.5}^{3+}\text{Bi}_{0.5}^{5+}][\text{Ni}^{2+}]$ configuration [43, 44]. Our calculated oxygen magnetic moment is large $\approx 0.1 \mu_B$, contrary to the expectation of non-magnetic O^{2-} for $[\text{Bi}_{1.5}^{3+}\text{Bi}_{0.5}^{5+}][\text{Ni}^{2+}]$ configuration. Total energy calculations show that Ni favors a G-type AFM order, in agreement with neutron diffraction [56].

At HP, the DFT calculation gives rise to a metallic solution, with dispersive bands crossing the Fermi level. Our DFT total energy calculations shows ferromagnetic Ni-Ni interactions; we therefore predict the HP metal should show ferromagnetic correlations. Analyzing the projected O- p DOS, we again find significant weight at the unoccupied part, reflecting the ligand hole. However, the unoccupied O- p states have lot more Ni- d character, and much less Bi- s character, compared to the AP phase. Interestingly, the magnetic moment on Ni site in the HP

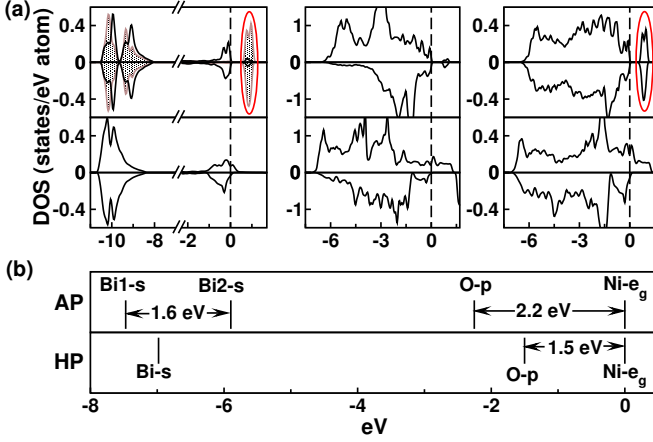


FIG. 2: (Color online) (a) GGA+ U projected DOS of BiNiO₃ in AP (top panels) and HP (bottom panels) phase. Left, middle, and right panels show projections to Bi- s (displaying relevant energy ranges), Ni- d , and O- p . Zero of energy is set at GGA+ U Fermi energies. For AP, projections to Bi1 (solid, black) and Bi2 (shaded) are shown separately. (b) Calculated energy levels of Bi- s , O- p and Ni- e_g in AP and HP phase. Zero of energy is set at Ni- e_g .

phase ($1.48\mu_B$) is not much smaller than in the AP phase ($1.73\mu_B$), in marked contrast to proposal of Ni²⁺ to Ni³⁺ valence transition between AP and HP. DFT thus suggests stabilization of $[\text{Bi}^{3+}\underline{L}^\delta][\text{Ni}^{2+}\underline{L}^{1-\delta}]$ configuration in the metal. This picture within single-reference description of DFT is close to the multi-reference description given by Ni K-edge X-ray absorption spectroscopy.[46] Calculation of crystal orbital Hamiltonian population (COHP) [64, 65] (see SM), corroborates the change of ligand hole character from Bi- s to Ni- d .

What causes this shift of oxygen covalency? To answer this, we show in Fig. 2(b), the computed Bi- s , Ni- e_g and O- p energy level positions in AP and HP phases, obtained from the low-energy tight-binding Hamiltonian in Wannier function basis within the N-th order muffin-tin-orbital (NMTO) formulation of downfolding technique [66, 67] (see SM). At AP, the s -level energy positions of Bi1 and Bi2, differ by about 1.5eV, Bi2- s being closer to O- p compared to Bi1- s , leading to stronger covalency between Bi2- s and O- p . Ligand holes are thus preferably associated with Bi2. At HP, the energies of Ni- d and O- p get markedly closer, driving a covalency shift to Ni-O.

Our DFT results for PbCrO₃ are qualitatively similar. The quantitative differences in PbCrO₃, a smaller critical pressure and larger volume collapse, arise from the O level lying closer to Pb. Thus, the Pb-O covalency is stronger than Bi-O. At the same time, Cr t_{2g} orbitals hybridize less effectively with O than Ni e_g (see SM).

Slave rotor theory. — In order to go beyond the DFT+ U treatment of strong correlation effect, and capture the Mott transition without any assumption of magnetic ordering, we next investigate such ABO₃ per-

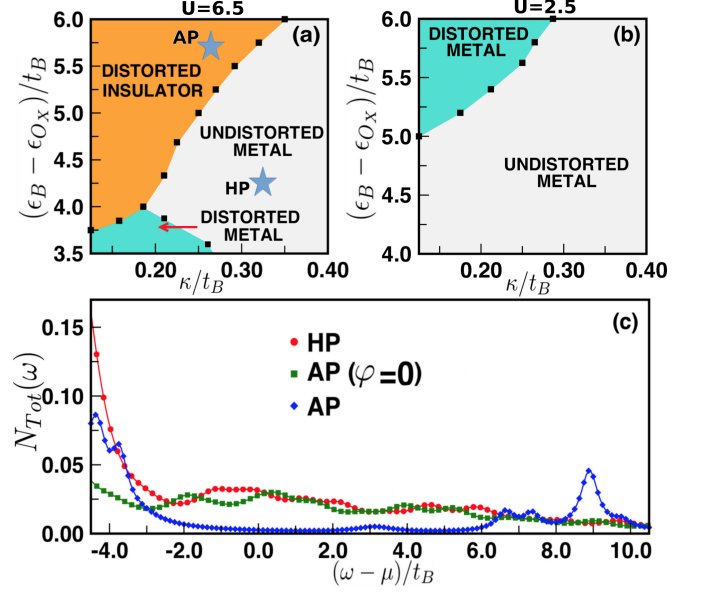


FIG. 3: (Color online) Phase diagram varying κ and $\epsilon_B - \epsilon_{Ox}$ for (a) $U/t_B = 6.5$ and (b) $U/t_B = 2.5$. (c) DOS $N_{\text{Tot}}(\omega)$ for typical points in AP and HP phases, marked by stars in (a), as well as DOS for metastable AP phase with imposed $\varphi = 0$.

ovskites in a DFT-inspired “ s - p - d ” model, which we study using slave rotor mean field theory [68–72]. Our work represents a novel application of slave-rotor which simultaneously treats all three ions (A, B, O). In contrast to previous work [43, 44], our model does not include a phenomenological *negative* U on the A-site. Instead, we include phonon distortion and A-O hybridization, which provides a more meaningful microscopic picture [73, 74].

Our model for ABO₃ consists of a multi-orbital manifold on the B-site, with non-degenerate orbitals on A and on the oxygen site. The on-site energies are denoted by ϵ_A , ϵ_B , and ϵ_{Ox} ; we fix $\epsilon_B = 0$. Denoting A-O and B-O hopping amplitudes in the symmetric phase as t_A , t_B respectively, and including a Hubbard $U > 0$ on B-site, yields the Hamiltonian $H = H_1 + H_2 + H_3 + H_4$, with

$$\begin{aligned}
 H_1 &= \epsilon_A \sum_{\mathbf{r}, \sigma} a_{\mathbf{r}+\Delta, \sigma}^\dagger a_{\mathbf{r}, \sigma} + \epsilon_{Ox} \sum_{\mathbf{r}, \sigma, \delta} \ell_{\mathbf{r}+\delta, \sigma}^\dagger \ell_{\mathbf{r}, \sigma} \\
 H_2 &= -t_B \sum_{\mathbf{r} \alpha \sigma \delta} g_{\alpha \delta} (b_{\alpha, \mathbf{r}, \sigma}^\dagger [\ell_{\mathbf{r}+\delta, \sigma} + \ell_{\mathbf{r}-\delta, \sigma}] + \text{h.c.}) \\
 &\quad + \frac{U}{2} \sum_{\mathbf{r}} \left(\sum_{\alpha \sigma} b_{\alpha, \mathbf{r}, \sigma}^\dagger b_{\alpha, \mathbf{r}, \sigma} - 2 \right)^2 \\
 H_3 &= -t_A \sum_{\mathbf{r}, \delta, \eta \delta, \sigma} [1 + \varphi(-1)^{\mathbf{r}}] (a_{\mathbf{r}+\Delta, \sigma}^\dagger \ell_{\mathbf{r}+\Delta+\eta \delta, \sigma} + \text{h.c.}) \\
 H_4 &= 12N \times \frac{1}{2} \kappa \varphi^2
 \end{aligned}$$

where a , b , ℓ denote electron operators on A, B, and ligand site respectively, with α labelling B-site orbitals. Here H_1 describes the on-site energy, with a choice $\epsilon_B = 0$, while H_2 and H_3 respectively describe the B-O and A-

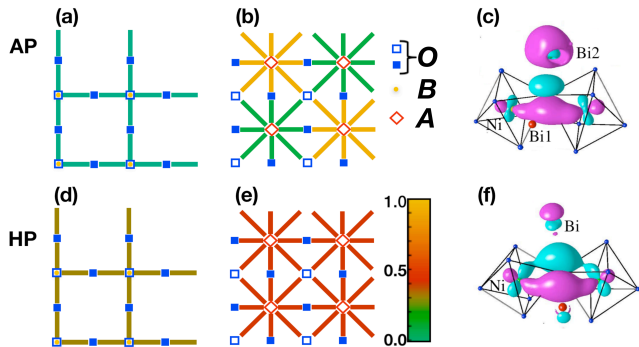


FIG. 4: (Color online) Bond-dependent kinetic energy from model (color bar shows magnitude) for B-O and A-O sublattices in AP ((a) and (b)) and HP ((c) and (d)) phase, projected to xy plane. Constant amplitude surfaces of DFT O- p Wannier functions for BiNiO₃ at AP (e) and HP (f), superposed on NiO₆ octahedra with adjacent two Bi ions. Cyan (light) and magenta (dark) colors indicate opposite signs.

O electronic Hamiltonians, and H_4 denotes the elastic energy cost of A-O bond deformations. Based on DFT, we assume the stiffer B-O sublattice to be immune to breathing distortion. Staggered A-O hopping, $t_A(1 \pm \varphi)$, permits us to capture the A-O *hybridization-wave*. In the symmetric phase $\varphi=0$. In the distorted phase $\varphi = \beta \frac{\delta a_{AO}}{a_{AO}}$, where $\beta \equiv (\partial \ln t_A / \partial \ln a_{AO})$, and δa_{AO} is the change in A-O bond length compared to its undistorted value a_{AO} . The elastic energy cost in H_4 is $\frac{1}{2} \kappa \varphi^2$ per bond, where $\kappa = k a_{AO}^2 / \beta^2$, with spring stiffness constant k , and $12N$ A-O bonds. For BiNiO₃, we have two e_g orbitals ($1 \equiv d_{x^2-y^2}$, $2 \equiv d_{3z^2-r^2}$) at the Ni-site, with $g_{1,x/y/z} = \{1, -1, 0\}$ and $g_{2,x/y/z} = \frac{1}{\sqrt{3}} \{-1, -1, 2\}$ due to orbital-dependent Ni to ligand hopping [75]. This model can be extended to study t_{2g} orbitals relevant to Cr in PbCrO₃.

We study the zero temperature phase diagram of Hamiltonian H using slave rotor mean field theory on the B-site (see SM for details). This approach ignores fluctuations of the rotor field as well as gauge fluctuations; nevertheless, it reasonably captures strong correlation effects [68–72]. We work in units with $t_B=1$. We choose $(\epsilon_A - \epsilon_B)/t_B = 8$, $t_A/t_B = 2.5$, and vary κ and ϵ_{Ox} , with $\epsilon_A < \epsilon_{Ox} < \epsilon_B$. Some variation in these parameters does not qualitatively affect our main results. Fig. 3 shows the phase diagram with varying ligand energy and stiffness κ , for a B-site ion with (a) $U/t_B = 6.5$, and (b) $U/t_B = 2.5$. For significant κ , when ϵ_{Ox} is close to ϵ_B , the ground state is an undistorted metal (UM) with non-integer B-site occupancy n_B . Tuning ϵ_{Ox} towards ϵ_A , or κ to smaller values, leads to a transition into either a distorted Mott insulator (DI) with pinned $n_B = 2$ (i.e., a “doping tuned” Mott transition on B site), or a distorted metal (DM), de-

pending on U . The strongly correlated case, $U/t_B = 6.5$, which results in a Mott localized DI, mimics the Ni site in BiNiO₃; for $t_B = 0.75eV$, we get $U \approx 5eV$. A spontaneous A-O hybridization-wave $\pm\varphi$ thus cooperates with the large U on the B-site, and results in this B-O to A-O *hybridization-switching induced Mott insulator*.

The critical value $(\epsilon_B - \epsilon_{Ox})_{crit}$ for the MIT increases with increasing κ . At the indicated point in the DI phase in Fig. 3(a), with $\kappa \approx 0.25$, the optimal distortion $\varphi \approx 0.55$. Choosing $\beta \approx 5$ [76] and $a_{BiO} = 2.3\text{\AA}$ yields $\delta a_{AO} \approx 0.25\text{\AA}$ as seen in BiNiO₃. Setting $t_B = 0.75eV$, we get $(\epsilon_B - \epsilon_{Ox})_{crit} \approx 3.8eV$ for metallization, while the κ value implies a stiffness $k \approx 1eV/\text{\AA}^2$, in reasonable agreement with DFT given the simplicity of the model which retains only Ni e_g and a single ligand orbital. The DOS, shown in Fig. 3 (c), displays a Mott gap in the DI phase while it is metallic in the UM phase. Forcing $\varphi = 0$ within the DI phase leads to a metallic DOS (see Fig. 3(c)); correlations alone are thus *insufficient* to induce an insulator.

Bond dependent hybridization. — Figs. 4 (a)-(d) shows the bond-dependent kinetic energy on the A-O and B-O bonds from the model Hamiltonian. In the DI phase, the B-O hybridization is weak, while AO₁₂ polyhedra display the hybridization-wave. In the UM phase, on the other hand, the B-O hybridization strengthens significantly compared to that in insulating phase, while the A-O hybridization becomes uniform. We corroborate this using NMTO-downfolding-derived DFT Wannier function plots of BiNiO₃ in O- p only basis calculations, as shown in Fig. 4(e), (f) [77]. At AP, the Wannier function is highly asymmetric, having a pronounced tail at Bi2 and nearly vanishing at Bi1. At HP, on the other hand, it is symmetric between Bi sites. Moving from AP to HP the tail at Ni is strengthened significantly, highlighting the change from Bi s -like to Ni d -like ligand hole.

Conclusion. — We have proposed the concept of a hybridization-switching induced Mott transition in ABO₃ perovskites, with BiNiO₃ and PbCrO₃ as concrete examples. Using DFT and slave rotor theory, we have identified its key ingredients as: (a) extended A-site orbitals, which strongly hybridize with oxygen to generate ligand holes and highly covalent A-O bonds susceptible to distortion, and (b) strong correlations on B-site ion. Pressure tuning the oxygen energy produces a volume-collapse Mott insulator to metal transition via shift in covalency. Based on our study, we propose TiMnO₃ [78, 79], and even $5s$ systems like InMnO₃, as further promising material candidates [80]. Charge doping such Mott insulators may lead to polaronic transport and superconductivity.

TS-D thanks the Department of Science and Technology, India for the support through Thematic Unit of Excellence. AP is supported by NSERC of Canada and the Canadian Institute for Advanced Research. ID is supported by Department of Science and Technology, India.

-
- * Electronic address: t.sahasgupta@gmail.com
- [1] N. F. Quackenbush, J. W. Tashman, J. A. Mundy, S. Sallis, H. Paik, R. Misra, J. A. Moyer, J.-H. Guo, D. A. Fischer, J. C. Woicik, D. A. Muller, D. G. Schlom, and L. F. J. Piper Nano Lett. **13** 4857 (2013).
 - [2] Elbio Dagotto, Science **309**, 257 (2005).
 - [3] A. V. Boris, Y. Matiks, E. Benckiser, A. Frano, P. Popovich, V. Hinkov, P. Wochner, M. Castro-Colin, E. Detemple, V. K. Malik, C. Bernhard, T. Prokscha, A. Suter, Z. Salman, E. Morenzoni, G. Cristiani, H.-U. Habermeier, B. Keimer, Science **332**, 937 (2011).
 - [4] Tae-Hwan Kim, M. Angst, B. Hu, R. Jin, X.-G. Zhang, J. F. Wendelken, E. W. Plummer, and An-Ping Li, PNAS, **107** 5272 (2010).
 - [5] Claudio Giannetti, Massimo Capone, Daniele Fausti, Michele Fabrizio, Fulvio Parmigiani, Dragan Mihailovic Advances in Physics, **65** 58 (2016).
 - [6] Masatoshi Imada, Atsushi Fujimori, and Yoshinori Tokura Rev. Mod. Phys. **70**, 1039 (1998).
 - [7] J. Zaanen, G. A. Sawatzky, and J. W. Allen, Phys. Rev. Lett. **55**, 418 (1985).
 - [8] K. Held, G. Keller, V. Eyert, D. Vollhardt, and V. I. Anisimov, Phys. Rev. Lett. **86**, 5345 (2001); N.F. Mott, Journal de Physique **42**, 277 (1981); N. F. Mott and L. Friedman, Phil. Mag.: A Journal of Theoretical Experimental and Applied Physics, **30:2**, 389 (1974).
 - [9] Z.-X. Shen, D. S. Dessau, Physica Reports 253, 1 (1995); M Kozielski, I Pollini and G Spinolo, J. Phys C: Solid State Phys, 5, 1253 (1972).
 - [10] J. B. Torrance, P. Lacorre, A. Nazzal, E. J. Ansaldo, and Ch. Niedermayer, Phys. Rev. B **45**, 8209(R) (1992).
 - [11] Enju Sakai, Masatomo Tamamitsu, Kohei Yoshimatsu, Satoshi Okamoto, Koji Horiba, Masaharu Oshima, and Hiroshi Kumigashira Phys. Rev. B **87**, 075132 (2013).
 - [12] J. Garcia-Munoz, et al, Europhys. Lett 20, 241 (1992).
 - [13] J. L. Garcia-Munoz, et al., Phys. Rev. B **50**, 978 (1994).
 - [14] J. Rogriguez-Carvajal, et al., Phys. Rev. B **57**, 456 (1998).
 - [15] M. T. Fernandez-Diaz et al., Phys. Rev. B **64**, 144417 (2001).
 - [16] D Meyers, et al, J. Phys. D: Applied Physics **46**, 385303 (2013).
 - [17] S. Middey, et al, Scientific Reports, 4, 6819 (2014).
 - [18] S. Catalano, et al, APL Materials 2, 116110 (2014).
 - [19] G. Berner, et al, Phys. Rev. B **92**, 125130 (2015).
 - [20] M. H. Upton, et al, Phys. Rev. Lett. **115**, 036401 (2015).
 - [21] E. Mikheev, A. J. Hauser, B. Himmetoglu, N. E. Moreno, A. Janotti, C. G. Van de Walle, and S. Stemmer, Sci. Adv. **1**, e1500797 (2015).
 - [22] V. Bisogni, et al, Nature Communications 7, 13017 (2016).
 - [23] Y. Lu, et al, Phys. Rev. B **93**, 165121 (2016).
 - [24] S. Middey, J. Chakhalian, P. Mahadevan, J. W. Freeland, A. J. Millis, and D. D. Sarma, Annual Review of Materials Research, **46**, 305-334 (2016).
 - [25] G. Fabbris et. al, Phys. Rev. Lett., **117**, 147401 (2016).
 - [26] J. Ruppen, et al, Phys. Rev. B **96**, 045120 (2017).
 - [27] I. Mazin, et al, Phys. Rev. Lett **98**, 176406 (2007).
 - [28] S.B. Lee, R. Chen, L. Balents, Phys. Rev. Lett. **106**, 016405 (2011).
 - [29] S.B. Lee, R. Chen, L. Balents, Phys. Rev. B **84**, 165119 (2011).
 - [30] Hyowon Park, Andrew J. Millis, and Chris A. Marianetti, Phys. Rev. Lett. **109**, 156402 (2012).
 - [31] Steve Johnston, Anamitra Mukherjee, Ilya Elfimov, Mona Berciu, and George A. Sawatzky, Phys. Rev. Lett. **112**, 106404 (2014).
 - [32] H. Park, A. J. Millis, C. A. Marianetti Phys. Rev. B **89**, 245133 (2014).
 - [33] E. A. Nowadnick, et al, Phys. Rev. B **92**, 245109 (2015).
 - [34] A. Subedi, O. E. Peil, and A. Georges, Phys. Rev. B **91**, 075128 (2015).
 - [35] R. J. Green, M. W. Haverkort, G. A. Sawatzky, Phys. Rev. B **94**, 195127 (2016).
 - [36] P. Seth, et al, Phys. Rev. B **96**, 205139 (2017).
 - [37] J. Varignon, M. N. Grisolia, J. Iniguez, A. Barthélémy, M. Bibes, NPJ Quantum Materials **2:21** (2017).
 - [38] S. Ishiwata, M. Azuma, M. Takano, E. Nishibori, M. Takata, M. Sakata, K. Kato, J. Mater. Chem. **12**, 3733 (2002).
 - [39] R. Yu et. al, J. Am. Chem. Soc., **137**, 12719 (2015).
 - [40] Note in case of BiNiO₃, Bi ion occupies the A-site, providing an intricate interplay between active A-site and the active strongly correlated B-site, namely Ni. This is unlike the case of BaBiO₃ (see e.g. Refs.[50–53]) in which the Bi ion, occupying the B-site, is at the center of the oxygen octahedra. For BaBiO₃, the structure and phenomenology is thus more similar to the rare-earth nickelates, with Ba cation not playing any active role.
 - [41] S. Ishiwata, M. Azuma, M. Hanawa, Y. Moritomo, Y. Ohishi, K. Kato, M. Takata, E. Nishibori, M. Sakata, I. Terasaki, and M. Takano Phys. Rev. B **72**, 045104 (2005).
 - [42] Masaki Azuma, Wei-tin Chen, Hayato Seki, Michal Czapski, Smirnova Olga, Kengo Oka, Masaichiro Mizumaki, Tetsu Watanuki, Naoki Ishimatsu, Naomi Kawamura, Shintaro Ishiwata, Matthew G. Tucker, Yuichi Shimakawa and J. Paul Attfield, Nat. Commun. **2:347** (2011).
 - [43] Makoto Naka, Hitoshi Seo, and Yukitoshi Motome Phys. Rev. Lett. **116**, 056402 (2016).
 - [44] Shoya Kojima, Joji Nasu, and Akihisa Koga, Phys. Rev. B **94**, 045103 (2016).
 - [45] P. Kuiper, G. Kruizinga, J. Ghijsen, G. A. Sawatzky, and H. Verweij Phys. Rev. Lett. **62**, 221 (1989).
 - [46] Masaichiro Mizumaki, Naoki Ishimatsu, Naomi Kawamura, Masaki Azuma, Yuichi Shimakawa, Mikio Takano, and Takayuki Uozumi, Phys. Rev. B. **80**, 233104 (2009).
 - [47] Izumi Hase and Takashi Yanagisawa, Phys. Rev. B **76**, 174103 (2007).
 - [48] K. Haule and G. L. Pascut, Sci. Rep. **7** 10375 (2017).
 - [49] A. Mercy, J. Bieder, J. Iniguez, P. Ghosez, Nat. Com. **8**, 1677 (2017).
 - [50] C. Franchini, A. Sanna, M. Marsman, and G. Kresse Phys. Rev. B **81**, 085213 (2010).
 - [51] C. Franchini, G. Kresse, and R. Podloucky Phys. Rev. Lett. **102**, 256402 (2009).
 - [52] Kateryna Foyevtsova, Arash Khazraie, Ilya Elfimov, and George A. Sawatzky Phys. Rev. B **91**, 121114(R) (2015).
 - [53] Arash Khazraie, Kateryna Foyevtsova, Ilya Elfimov, and George A. Sawatzky Phys. Rev. B **97**, 075103 (2018).
 - [54] Y. Ishige, T. Sudayama, Y. Wakisaka, T. Mizokawa, H. Wadati, G. A. Sawatzky, T. Z. Regier, M. Isobe, and Y. Ueda Phys. Rev. B **83**, 125112 (2011).
 - [55] P.A. Bhoobe, A. Kumar, M. Taguchi, R. Eguchi, M. Matsumami, Y. Takata, A.K. Nandy, P. Mahadevan, D.D.

- Sarma, A. Neroni, E. aolu, M. Leai, M. Oura, Y. Senba, H. Ohashi, K. Ishizaka, M. Okawa, S. Shin, K. Tamasaku, Y. Kohmura, M. Yabashi, T. Ishikawa, K. Hasegawa, M. Isobe, Y. Ueda, and A. Chainani Phys. Rev. X **5**, 041004 (2015).
- [56] Masaki Azuma, Sandra Carlsson, Jennifer Rodgers, Matthew G. Tucker, Masahiko Tsujimoto, Shintaro Ishiwata, Seiji Isoda, Yuichi Shimakawa, Mikio Takano, and J. Paul Attfield, J. Am. Chem. Soc., **129**, 14433 (2007).
- [57] J. P. Perdew, K. Burke, and M. Ernzerhof, Phys. Rev. Lett. **77**, 3865 (1996).
- [58] V. I. Anisimov, I. V. Solovyev, and M. A. Korotin, Phys. Rev. B **48**, 16929 (1999).
- [59] G. Kresse et. al., Phys. Rev. B **54**, 11169 (1996).
- [60] The supplemental material contains detailed information regarding: (i) crystal structures, (ii) DFT computations, (iii) results of COHP calculations, and (iv) formalism and results of slave-rotor mean field theory.
- [61] F. Birch, Phys. Rev. **71**, 809 (1947).
- [62] M. Medarde, C. Dallera, M. Grioni, B. Delley, F. Vernay, J. Mesot, M. Sikora, J. A. Alonso, and M. J. Martinez-Lope, Phys. Rev. B **80** 245105 (2009).
- [63] We find the charge difference between Bi1-s and Bi2-s to be rather small ($< 2\%$) for choice of three different basis sets, LMTO, LAPW and plane-wave. In case of LMTO, overlapping spheres are used, while in case of LAPW and plane-wave calculations non-touching spheres are used. The consistency of results in three different basis sets conclusively shows negligible charge disproportionation between two Bi, rather it arises in the intervening O ion. We contrast this with manganites, where the charge difference at two Mn sites, increases from from the smallest value of 8% for the single layer compound to 39% for the double layer material, and to 22 % for the infinite layer compound (Phys. Rev. B **80** 064402 (2009)).
- [64] R. Dronskowski, P. E. Blöchl, J. Phys. Chem. **97**, 8617 (1993).
- [65] F. Boucher, R. Rousseau, Inorg. Chem. **37**, 2351 (1998).
- [66] O. K. Andersen and T. Saha-Dasgupta, Phys. Rev. B **62**, R16219 (2000).
- [67] Ni- t_{2g} being fully filled in both AP and HP phases, they have not been considered. The small, but finite splitting between the two e_g levels of Ni, and three p levels of oxygen due to finite distortion is not shown for simplicity. Also there is some variation between energy levels of different inequivalent Ni's (in case of AP) and different inequivalent O's. Only the averaged positions are shown.
- [68] S. Florens and A. Georges, Phys. Rev. B **66**, 165111 (2002).
- [69] S. Florens and A. Georges, Phys. Rev. B **70**, 035114 (2004).
- [70] B. Lau and A. J. Millis, Phys. Rev. Lett **110**, 126404 (2013).
- [71] S. S. Lee and P. A. Lee, Phys. Rev. Lett. **95**, 036403 (2005).
- [72] E. Zhao and A. Paramakanti, Phys. Rev. B **76**, 195101 (2007).
- [73] C. M. Varma, Phys. Rev. Lett, **61**, 2713 (1988).
- [74] W. A. Harrison, Phys. Rev. B **74**, 245128 (2006).
- [75] J. C. Slater and G. F. Koster, Phys. Rev. **94**, 1498 (1954).
- [76] G. Grosso and C. Piermarocchi, Phys. Rev. B **51**, 16772 (1995).
- [77] The Wannier functions are constructed by NMTO-downfolding technique, in which only O- p degrees of freedom are kept active in the basis, rest including Ni- d and Bi- s degrees of freedom being downfolded.
- [78] Wei Yi, Yu Kumagai, Nicola A. Spaldin, Yoshitaka Matsushita, Akira Sato, Igor A. Presniakov, Alexey V. Sobolev, Yana S. Glazkova, and Alexei A. Belik, Inorg. Chem. **53**, 9800 (2014).
- [79] The ambient condition crystal structure of TlMnO₃ reported in literature [78] has triclinic symmetry with two inequivalent Tl positions. Although the valence of Tl was assumed to be nominally 3+, the first-principles calculation reported in [78] shows that the energies of the formally 'unoccupied' Tl 6s states are substantially lower than expected. Thus the Tl 6s states, which would be completely empty in the ionic limit, develop significant occupation through Tl-O covalency and form the bottom of the valence band. The situation is thus analogous to BiNiO₃, and a hybridization wave would result in a lower symmetry structure with two inequivalent Tl sites. The case of TlMnO₃ should thus be revisited in light of our findings, to explore the effect of pressure, temperature, and isovalent substitution on Tl site.
- [80] Note that discussed cases are different in behavior from that of BiFeO₃ or PbTiO₃, the so-called magnetic ferroelectric compounds, though they also possess A site with extended 6s orbital. What makes BiFeO₃ or PbTiO₃ different from BNO or PCO, is the absence of ligand hole in the former and presence of ligand hole in the later. Both BNO and PCO are in negative-charge transfer situation at AP, thereby creation of ligand hole in A-O sublattice, and subsequent ligand-hole driven hybridization wave. Unlike this, though the finite A-O covalency in case of BiFeO₃ or PbTiO₃ drives the stereochemical activity of A sites, it is not sufficiently strong to drive the negative charge transfer situation.